Natural and Anthropogenic Influences on the Mount Hope Bay Ecosystem
2006 *Northeastern Naturalist* 13(Special Issue 4):117–144

The Exchange of Water through Multiple Entrances to the Mount Hope Bay Estuary

Chris Kincaid*

Abstract - Results are presented from a set of hydrographic surveys conducted within Mount Hope Bay, RI, during the summer of August, 1996. This sub-system of Narragansett Bay is interesting because it has two connections to the ocean and it has a source of thermal energy from the Brayton Point Power Plant. Data was collected on water velocity, salinity and temperature on days with relatively high (≈ 2 m range) and relatively low (≈ 1 m range) tidal forcing. Velocity data were collected along fixed transect lines defining the boundaries of the estuary and at fixed stations. Results show that flow through each of the oceanward entrances has significant horizontal and vertical structure. The source of fresh water is the Taunton River to the north, and at times, exchange through this interface exhibits vertically sheared flow. Exchange is dominated by flow through the interface with Narragansett Bay, where transports reach 3000 m^3/s and 6000 m^3/s under conditions of low and high amplitude tidal forcing, respectively. Peak velocities exceed 100 cm/s. Values for transport though the smaller of the two salt water connections, with the Sakonnet River, and the fresh water entrance, at the interface with the Taunton River, were ≈ 10– 20% of those through the interface with Narragansett Bay. Velocities are relatively sluggish in the shallow northern shelf region of the estuary, peaking at < 10 cm/s and ≈ 20 cm/s for the low and high tidal amplitude sampling periods, respectively. Temperature and salinity data reveal significant levels of stratification and suggest three end-member water sources including a deep Narragansett Bay source (cold, salty), a shallow river source (warm, fresh) and a source of water from the Brayton Point region (hot, intermediate salinity). A plug of warm water that evolves on the northern shelf over the ebb cycle of the tide is advected to the east–northeast into the shipping channel during the flood. Phase differences in total instantaneous transport through the two mouths of the system suggest that interactions with the Sakonnet River are dominated by the greater volume and efficiency of exchange with the East Passage of Narragansett Bay. Lateral variations in residual transport show East Passage water entering Mount Hope Bay through the deep central portion of the cross-section and exiting through confined regions along the edges of the interface. The pattern in residual exchange with the Sakonnet River shows water exiting and entering Mount Hope Bay through the western and eastern portions of the cross section, respectively. A conceptual model is suggested in which these lateral flow patterns combine with strong vertical mixing in the Sakonnet River Narrows to pump thermal energy downward in the water column and back northward into the bottom waters of Mount Hope Bay.

Introduction

Narragansett Bay represents an important ecosystem and resource for the states of Rhode Island and Massachusetts. Stress levels on the Narragansett

*Graduate School of Oceanography, University of Rhode Island, South Ferry Road, Narragansett, RI 02882; kincaid@gso.uri.edu.

Bay estuary have been rising. The system is experiencing a period of warming as evidenced by increasing winter–spring temperature (T) (by as much as 2 °C) that has been attributed to climate trends (Hawk 1998). Recent field surveys show that the upper portion of the estuary is subject to periods of chronically low dissolved oxygen (DO) and eutrophication (Deacutis 1999). Results from intensive summertime sampling through the Narragansett Bay Estuarine Program at 75 stations within the upper half of Narragansett Bay suggest that residence times within key regions of the upper Bay, rather than simply stratification levels, contribute to the evolution of hypoxic events.

The geometry of the estuary is complex. The entrance is composed of two distinct north–south oriented branches referred to as the East and West Passages. The upper Bay is comprised of three distinct sub-regions: Greenwich Bay, the Providence River, and the Mount Hope Bay (MHB) estuary. Mean depths in this system are relatively shallow, ranging from 7.6 to 10 m (Pilson 1985a). The deepest portion is the East Passage, with a mean water depth of 18 m and a maximum water depth of > 40 m. Freshwater enters the upper Bay through the Providence River, which is fed by the Blackstone and Pawtuxet Rivers. Another important freshwater source is through MHB, which is fed by the Taunton River (Fig. 1). The total discharge typically varies between a minimum of 20 m^3/s in late summer–fall to greater than 300 m^3/s under peak runoff conditions during the winter–spring months (Pilson

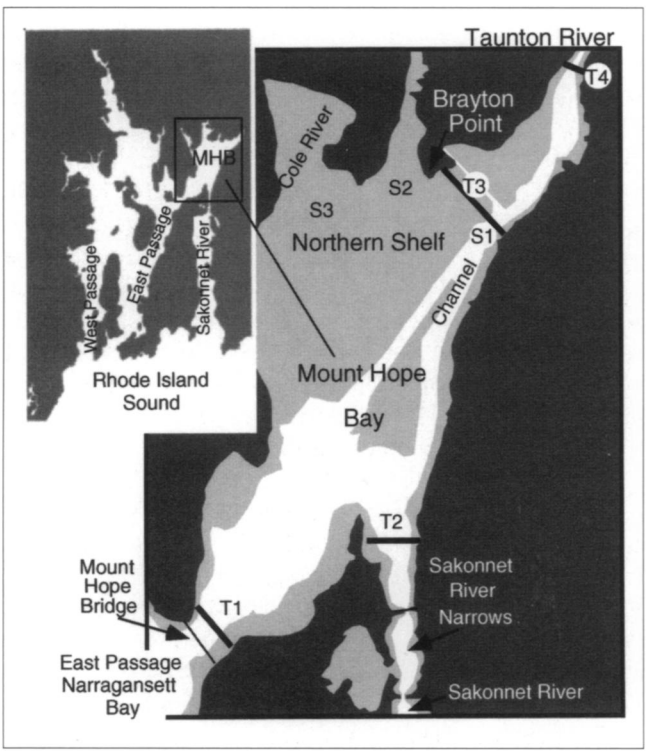

Figure 1. Map of the Mount Hope Bay (MHB) estuary showing the locations of the ADCP transect lines that cross the entrances to MHB (T1, T2, and T4). Another transect line crosses near Brayton Point (T3). Symbols S1, S2, and S3 mark locations where time series data were collected. The inset shows the location of MHB relative to Narragansett Bay.

1985a). The MHB system is of particular interest because it has two connection pathways to the ocean, one through the East Passage and the other through the Sakonnet River via the highly constricted and turbulent Sakonnet River Narrows (SRN) (Levine and Kenyon 1975; Fig. 1).

Over the past 40 years, numerous studies have focused on the physical, biological and chemical processes within the Narragansett Bay system (Hicks 1959; Keller et al. 1999; Pilson 1985a,b). Narragansett Bay is characterized as a partially to well-mixed estuary (Goodrich 1988) that is subject to strong tidal and wind forcing (Weisburg and Sturges 1976). Maximum vertical salinity (S) gradients have been estimated to be 2–3 psu (Goodrich 1988, Hicks 1959). Previous modeling and observational studies have focused on the tidal and wind driven flow (Deleo 2001, Gordon and Spaulding 1987, Hicks 1959, Levine and Kenyon 1975, Spaulding and White 1990, Weisberg 1976, Weisberg and Sturges 1976). Circulation in the upper Bay has been shown to be driven in roughly equal parts by tidal and wind forcing (Weisburg 1976). Previous studies also show that wind effects can permeate the entire water column, highlighting the importance of the wind in net estuarine circulation and transport patterns in Narragansett Bay (Weisberg 1972, 1976; Weisberg and Sturges 1976).

Results of the recent intensive summertime DO sampling in upper Narragansett Bay underscore the importance of constraining circulation patterns within and exchange between distinct sub-regions of the estuary through a combination of observational and modeling work. Gordan and Spaulding (1987) used a vertically integrated model to show that wind and tidal forcing combine to produce a range of flow patterns between subsections of the Bay. Physical measurements within Narragansett Bay have primarily utilized moored current meters at a limited number of locations (Rosenberger 2001, Shonting 1969, Spaulding and White 1990, Weisberg and Sturges 1976). In our study, we focus on the sub-region of MHB, which presents an interesting contrast to other regions of the upper Bay, i.e., Greenwich Bay and the Providence River. Data from current meter moorings within MHB show that the system is dominated by the M_2 tide at 80–90% of the energy, with a small contribution at the M_4 frequency that gives rise to a double-peaked flood and a single-peaked ebb (Spaulding and White 1990). Tidal amplitudes (e.g., half the total tidal range) vary from $\approx$ 40 cm at neap conditions to $\approx$ 80 cm for spring tides. The system exhibits characteristics of a standing wave, with currents out of phase with variations in surface elevation by 3 hours. Maximum tidal currents of 20 cm/s, 22 cm/s, and 4.5 cm/s have been reported by Spaulding and White (1990) for locations near our lines T1, T4, and T2, respectively (Table 1). More recent time series data on water level variations across the SRN reveal aspects of the temporal variability in exchange between the MHB and Sakonnet River systems (Deleo 2001).

We present data from hydrographic surveys conducted within MHB during summer, or stratified seasonal conditions. We utilized underway acoustic

Doppler current profiler (ADCP) measurements to characterize both spatial patterns in circulation within MHB and temporal patterns in exchange through MHB's two oceanward connections, with the East Passage of Narragansett Bay and the Sakonnet River (Fig. 1). A number of recent underway ADCP surveys have provided detailed spatial images of circulation through the mouths of major estuaries (Valle-Levinson and Lwiza 1995; Valle-Levinson et al. 1996, 1998; Wong and Münchow 1995), including Narragansett Bay (Kincaid et al. 2003). Our results show that flow through each of the salt water interfaces (T1 and T2 in Fig. 1) exhibits significant lateral structure. Layered flow is recorded through the freshwater interface at line T4, which is consistent with the findings of Spaulding and White (1990). However, peak velocities of > 100 cm/s and 50–60 cm/s are significantly higher than previously reported for the interface with the East Passage (T1) and at the head of the system (T4), respectively. Volume flux, or transport data through each interface, shows the dominant exchange pathway to be through the connection with the East Passage. Transport through the SRN is 10% of that through line T1 and is seen to reverse direction late in the flood and ebb stages of the tide, possibly in response to more efficient filling/flushing that occurs though the T1 boundary (Deleo 2001). Profiles of S and T show that water properties within MHB may be explained by mixing between three distinct end-member sources. The combined data set provides important constraints for three-dimensional hydrodynamic models of flow, transport, and residence time within Narragansett Bay (Bergondo et al. 2003).

Methods

This study utilized a ship-mounted ADCP in combination with conductivity, temperature, and depth (CTD) profiles. Circulation patterns and energies were recorded with an RD Instruments Broadband (1200 kHz) ADCP that was mounted to the side of a 20' skiff. ADCP data were collected along four distinct transect lines shown in Figure 1. Two of these lines define boundaries with water bodies that connect through to the ocean, including one along the interface with the East Passage of Narragansett Bay, beneath the Mount Hope Bridge (T1) and another along the interface between MHB and the Sakonnet River (T2) (Fig. 1, Table 1). Water depths exceed 25 m along the centerline of T1 and are closer to 16 m at the deepest (eastern) portion of T2. A third

Table 1. Summary of ADCP transect and time series station locations.

Name	Latitude (start)	Longitude (start)	Latitude (end)	Longitude (end)	Transect length (m)	Area (m^2)	Sampling time (min)
T1	41°38' 39"	-71°15'29"	41°38'12"	-71°15'13"	850	9550	10
T2	41°39'02"	-71°13'11"	41°38'58"	-71°12'31"	850	6200	10
T3	41°41'48"	-71°10'48"	41°42'28"	-71°11'24"	1450	16000	20
T4	41°43'21"	-71°09'16"	41°43'28"	-71°09'27"	290	2700	5
S1	41°41'54"	-71°10'56"					5
S2	41°42'26"	-71°11'56"					5
S3	41°42'25"	-71°13'10"					5

transect (T4) defines the approximate boundary between MHB and the Taunton River (T4). A relatively narrow region of deeper water runs northeasterly from line T1, eventually necking down into the shipping channel that continues along this trend towards line T4 and the Taunton River. To the north and northwest of the shipping channel lies a broad, shallow region, referred to here to as the northern shelf. A final line (T3) extends across the northern shelf from the vicinity of the Brayton Point Power Plant at its northwestern end to the shipping channel at the southeastern end of the transect. Data ensembles were collected along transect lines with a ping interval of 7 seconds. The average boat speed was 1 m/s; hence, velocity ensembles were collected every 7 m along track.

Measurements were also collected at fixed stations, where the vessel position was held constant and ADCP data were recorded continuously over a 5-minute time interval. These time series measurements were made at locations (Table 1) designated S1, S2, and S3 in Figure 1. Station S1 is in the center of the shipping channel at the southeastern end of T3, near buoy GC11. The other sites, labeled S2 and S3, were located on the northern shelf to the south and southwest of the Brayton Point Plant. Hydrographic profiles were made using a Seabird Seacat 19 CTD at each of the time series sites and at the mid-points of the transect lines. In the case of transect T3, the CTD casts were taken within the shipping channel.

Measurements were made on each cruise over a 13-hour period to capture both ebb and flood stages of the semi-diurnal tidal oscillation. Two cruises were selected to cover periods of relatively low- and high-amplitude tides. Figure 2 shows the tidal variation within upper Narragansett Bay from Providence, RI, for the two sampling days (August 22 and 29, 1996). During the cruises, ADCP and CTD data were collected along each transect line in sequence, followed by sampling at the time series locations. A complete set of measurements, or a circuit, generally required 2.25 hours.

A number of processing steps were performed to improve ADCP data quality and to highlight both instantaneous and residual circulation

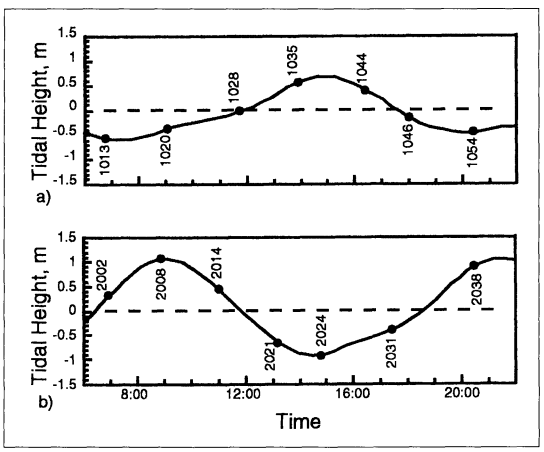

Figure 2. Variation in tidal height at Providence, RI, for the two survey days (a) August 22, 1996, and (b) August 29, 1996. Numbers on the plot show the relative timing of ADCP files for line T1 (listed in Tables 2 and 3).

patterns in the study area. The raw ADCP data included bad ensembles that appeared as obvious vertical stripes in contour plots of velocity magnitude and direction, most often associated with acceleration of the instrument due to wave activity. In particular, the afternoon sea breeze from the southwest induced significant wave energy in MHB. A low-pass median filter was used to remove these bad bins, as described in Kincaid et al. (2003). A range of filter window widths was investigated, from 4–11 data values. A comparison of values for integrated or total transport (Q in m^3/s) through each transect shows the different filters agree to within ≈ 10%. However, values for Q calculated from filtered data are consistently lower (by ≈ 5–15%) than those determined using the unfiltered data. Results on instantaneous and residual flows are presented from filtered data that has been processed with a median filter window of 5 data values, or ensembles, which corresponds to ≈ 30 m in width.

A number of methods have been used to estimate residual or non-tidal transport (q_R) from shipboard ADCP data (Candela et al. 1990, 1992; Foreman and Freeland 1991; Geyer and Signell 1990; Munchow et al. 1992; Simpson et al. 1990). In our analysis, residual transport is calculated within distinct lateral and vertical sub-sections within each transect in order to characterize spatial patterns in net exchange between MHB and neighboring bodies of water. The filtered velocity data were rotated into a transect-normal component, where positive values correspond to northward flow into the MHB or, in the case of line T4, northeastward flow into the Taunton River (Fig. 1). Times for individual transects are related to a dimensionless tidal stage by comparing the start time (t_s) of each transect relative to the predicted times for low tide at Providence, RI. Normalized transect start time, t^*, was calculated using $t^* = (t_s - t_1) / (t_2 - t_1)$, where t_1 and t_2 are the times of predicted low water before and after a particular survey, respectively (Tables 2 and 3).

The sampled portion of each transect was divided into subregions covering the upper and lower halves of the cross section and these were then sub-sectioned into 10 lateral bins of equal width. Values for instantaneous transport integrated for each bin were calculated as a function of t^* using the expressions

$$Q_s(k,t^*) = \sum_{i(k)}^{i(k+1)-1} \sum_{j=1}^{B(i)/2-1} u_{i,j}\, dx_i\, dz \qquad (1)$$

and

$$Q_B(k,t^*) = \sum_{i(k)}^{i(k+1)-1} \sum_{j=B(i)/2}^{B(i)} u_{i,j}\, dx_i\, dz \qquad (2)$$

where $u_{i,j}$ is the filtered, transect-normal velocity for each ADCP data point (i = columns or ensembles; j = ADCP depth cell number) and dz and dx_i are the height (50 cm) and width (≈ 7 m) of each ADCP cell. The lateral boundaries of each subsection (k) are given in the first summation. The

number of vertical ADCP cells ($B[i]$) is a function of position along track. Within the shallower set of bins (Q_s), velocity information is integrated from the surface ADCP cell down to one bin above the mid-depth level. The series of bottom subsections (Q_b) accumulates information from mid-depth down to the bottom ADCP cell. A residual transport was next determined for each

Table 2. Summary of ADCP and CTD data from survey day 1: August 22, 1996.

File (MHB)	Transect	Time (end)	Transport (m^3/s)	Flow direction (deg.)*	Flow magnitude (cm/s)	Tidal stage (0.1 = low, 0.5 = high)	
1013	T1	6:50	-1375			-0.05372	
1014	T2	7:20	330			-0.01343	
1015	T3	8:04	170	C: 270 (55); S: 50	C: 12 (12); S: 5	0.045662	Low water
1016	T4	8:15	245			0.060435	
1017	S1	8:27		300 (80)	5 (26)	0.076551	
1018	S2	8:39		125	9	0.092667	
1019	S3	8:50		60	6	0.10744	
1020	T1	9:13	1590			0.13833	
1021	T2	10:21	-190			0.22965	
1022	T3	10:41	725	C: 90 (90); S: 340	C: 5 (17); s:7	0.25651	
1023	T4	10:55	150			0.27532	Mid-flood
1024	S1	11:06		10 (60)	2 (20)	0.29009	
1025	S2	11:18		60 (135)	8 (2)	0.3062	
1026	S3	11:25		10 (60)	6 (6)	0.31561	
1028	T1	11:48	1890			0.34649	
1029	T2	12:08	250			0.37335	
1030	T3	12:38	1050	C:70; S:50	C:20; S:7	0.41364	
1031	T4	12:55	720			0.43648	
1032	S1	13:09		80	31	0.45528	
1033	S2	13:18		110	8	0.46737	
1034	S3	13:23		60	5	0.47408	
1035	T1	13:49	3070			0.509	
1036	T2	14:17	-150			0.5466	High water
1037	T2S	14:22		340 (225)	6 (15)	0.55332	
1039	T3	15:02	100	C:180 (80); S:180	C:8 (8); S:8	0.60704	
1040	S1	15:13		270 (90)	7 (7)	0.62181	
1041	T4	15:19	-35			0.62987	
1042	S2	15:44		90	7	0.66344	
1043	S3	15:57		45 (200)	8	0.6809	
1044	T1	16:34	-2950	230	30	0.73059	Mid-ebb
1045	T2	17:37	-170			0.8152	
1046	T1	18:01	-3330			0.84743	
1047	T3	18:34	-900	C:250(250); S:270	C:32(10); S:12	0.89175	
1049	T4	18:54	-510			0.91861	
1050	S1	19:16		270 (180)	26 (5)	0.94816	
1051	S2	19:25		135	5	0.96025	
1052	S3	19:31		120	5	0.96831	
1053	T2	19:57	410			1.0032	
1054	T1	20:22	0			1.0368	Low water

*For time series and line T3 we summarize average flow directions (given in degrees from north) and magnitudes within the upper and lower halves of the water column. Symbols C and S for line T3 denote values within the channel and on the northern shelf. Values for lower portion of the water column are included in parentheses. If there are no parentheses, the surface and bottom values for both magnitude and direction are equal.

of the subdivisions (k) across a transect by removing the tidal variation from the instantaneous transport data using a curve-fitting procedure expressed as

$$q(k,t^*) = q_R(k) + \sum_{m=1}^{3} a_m \sin(2\pi m t^* - \theta_m) \quad (3)$$

where q_R is residual transport [m^3s^{-1}], and a_m (θ_m) is the amplitude (phase) for each individual harmonic (m). Values for q_R were calculated by finding the combination of parameters that minimized the RMS difference (E) between the best-fit curve and measured transports using

Table 3. Summary of ADCP and CTD data from survey day 2; August 29, 1996.

File (MHB)	Transect	Time (end)	Transport (m^3/s)	Flow direction (deg.)*	Flow magnitude (cm/s)	Tidal stage (0.1 = low, 0.5 = high)	
2001	T2	6:34	475			0.36798	Mid-flood
2002	T1	7:02	5950			0.40559	
2003	T3	7:39	2050	C: 80; S: 80	C: 30; S: 27	0.45528	
2004	T4	7:54	1260			0.47542	
2005	S2	8:06		90	9	0.49154	
2006	S3	8:12		45	15	0.4996	
2007	T5	8:33				0.5278	
2008	T1	8:52	2160			0.55332	High water
2009	T2	9:13	-590			0.58152	
2010	T3	9:41	-225	C: 240 (50); S: 270	C: 12 (9); S: 8	0.61912	
2011	T4	9:57	-670			0.64061	
2012	S2	10:10		20 (180)	4 (4)	0.65807	
2013	S3	10:20		240	9	0.6715	
2014	T1	10:48	-4650			0.70911	
2015/16	T2	11:20	-325			0.75208	Mid-ebb
2017	T3	12:02	-1650	C: 270 (270); S: 270	C: 40 (22); S: 17	0.80849	
2018	T4	12:22	-950			0.83535	
2019	S2	12:35		200	9	0.85281	
2020	S3	12:48		200	15	0.87027	
2021	T1	13:18	-4000			0.91056	
2022/23	T2	13:42	330			0.94279	
2024	T1	14:52	-380			1.0368	Low water
2025	T2	15:17	370			1.0704	
2026	T3	15:53	825	C: 90; S: 90	C: 15; S: 15	1.1187	
2027	T4	16:19	560			1.1536	
2028	S2	16:35		100	17	1.1751	
2029	S3	16:45		50	8	1.1886	
2031	T1	17:30	2040			1.249	
2032	T2	17:55	320			1.2826	
2033	T3	18:30	1000	C: 80; S: 90	C: 15; S: 20	1.3296	Mid-flood
2034	T4	18:46	900			1.3511	
2035	S2	19:00		80	15	1.3699	
2036	S3	19:06		35	17	1.3779	
2038	T1	19:46	5130			1.4316	
2039	T2	20:13	250			1.4679	High water

*For time series and line T3 we summarize average flow directions and magnitudes within the upper and lower halves of the water column. Symbols C and S for line T3 denote values within the channel and on the northern shelf. Values for lower portion of the water column are included in parentheses. If there are no parentheses, the surface and bottom values for both magnitude and direction are equal.

$$E(k) = \left[\frac{1}{N} \sum_{n=1}^{N} [Q_s(k,t^*(n)) - q(k,t^*(n)]^2 \right]^{1/2} \quad (4)$$

in which N represents the total number of data points for an individual transect line. The three harmonics used in this analysis correspond to the M_2, M_4, and M_6 tidal frequencies. Error values correspond to a standard deviation about a best-fitting curve. The ADCP does not sample the upper 2 m or the bottom 1 m of the water column, so our calculated transports represent lower bound values. The missed data coverage is considered to be a problem only for determining residual flows for line T4 due to the strong, near-surface vertical gradients in velocity observed in this region.

Results

Exchange patterns though the mouths of MHB

Contours of instantaneous velocities provided by the ADCP reveal horizontal and vertical variability in flow through each of the entrances to MHB. Figure 3 shows two-dimensional patterns in flow through line T1 over the course of the tidal cycle during both of the sampling days. Early in the flood (Fig. 3b), water moves weakly (< 30 cm/s) into MHB through most of the cross-section. The inflow intensifies during this early stage of the flood in the lower and southeastern portion of the cross-section. An interesting feature of this data set is the region of stagnant or weakly ebbing water (Fig. 3b) that develops during this stage of the flood at the northwestern end of the cross section (e.g., at the bottom between 100 and 200 m along transect). As the flood progresses (Fig. 3c), the region of higher inflow expands upward in the water column forming a vertically uniform zone extending from just northwest of the deepest part of the channel to the shallow region at the southeastern end of the line (or from ≈ 200–600 m along transect). The zone of confined outflow at the northwestern end of T1 (e.g., < 200 m along transect) evolves into a region of weak inflow or stagnant water that increases in cross-sectional area towards the end of the flood (Fig. 3d).

Maximum inflow velocities are roughly 60 cm/s through T1 and are recorded 1 hour prior to high water. Assuming these are the maximum flood currents, the system appears to behave more as a progressive wave, characteristic of a frictionally dominated estuary, rather than a standing wave, where maximum flood currents occur midway between low and high water. Given the spacing in temporal sampling of our surveys, it is not clear that we captured maximum inflow. However, if peak inflow occurred after our sampling at 13:49 (Fig. 3d), this is also consistent with a characterization of a progressive wave, at least for flow at T1. During the ebb, the pattern in instantaneous flow through T1 evolves to more laterally continuous or uniform southwestward flow out of MHB over the entire cross-section. Maximum flow rates during the ebb are 50–60 cm/s.

There are a number of interesting differences and similarities in flow patterns through T1 between the two survey days. The most obvious impact of the larger tidal amplitude on survey day 2 is that maximum inflow rates exceed 100 cm/s over much of the cross-section during peak flood (Fig. 3h). However, comparisons between T1 cross-sections from similar tidal stages

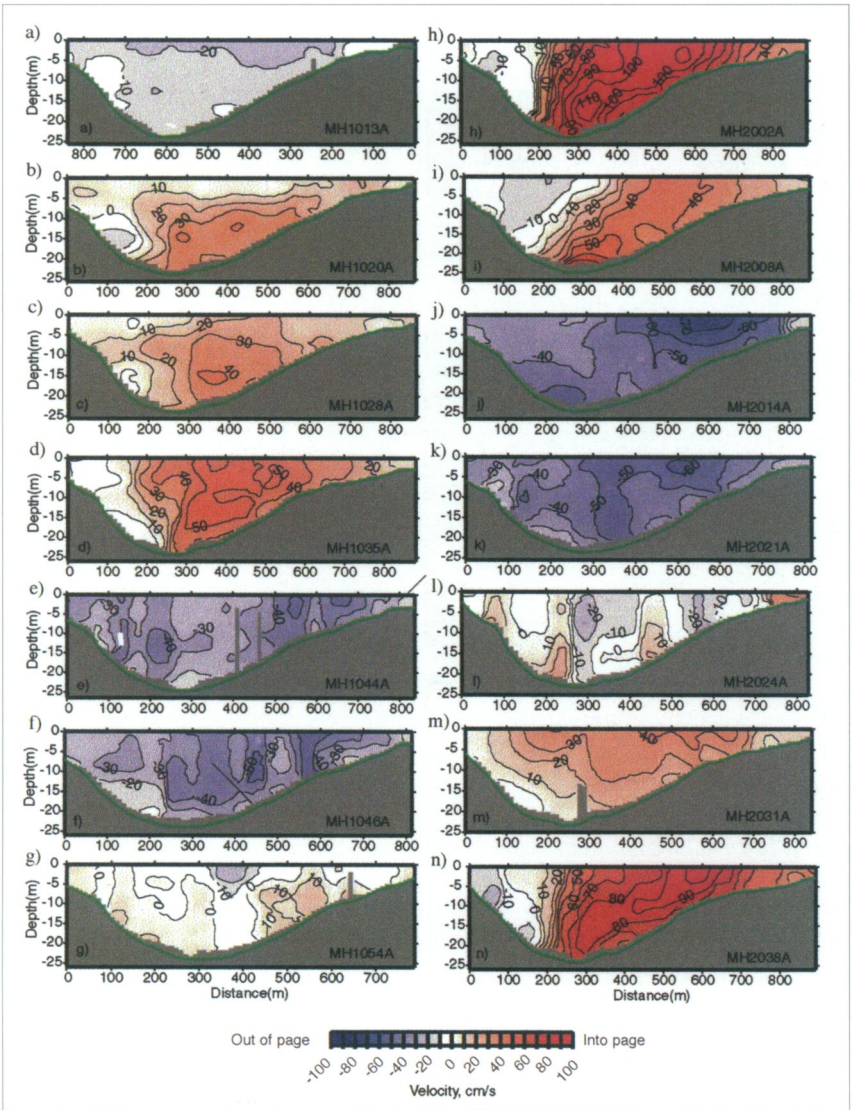

Figure 3. Contour plots of velocity magnitude normal to transect line T1. Colors correspond to flow rates listed in the scale bar. Reds represent flow to the northeast, or currents entering MHB. Blues represent flow out of MHB, to the southwest. The cross-section is oriented with northwest to the left and southeast to the right, as viewed looking into MHB from the East Passage. Frames (a–g)are from the first survey day. Frames (h–n) are from the second survey day.

highlight differences in the spatial evolution of the inflow to MHB given the two tidal amplitudes. Velocity contours for the T1 cross-section for sampling day 2 (≈ 2-m tide) are shown in Figures 3h–n. As opposed to survey day 1, where inflow intensified deep in the water column, during the early flood period on August 29, the inflow intensified more in the upper portion of the water column (Fig. 3m). During mid-flood stage of the tide (Fig. 3h) through to the later stages of the flood (Fig. 3n, 3i), the zone of maximum

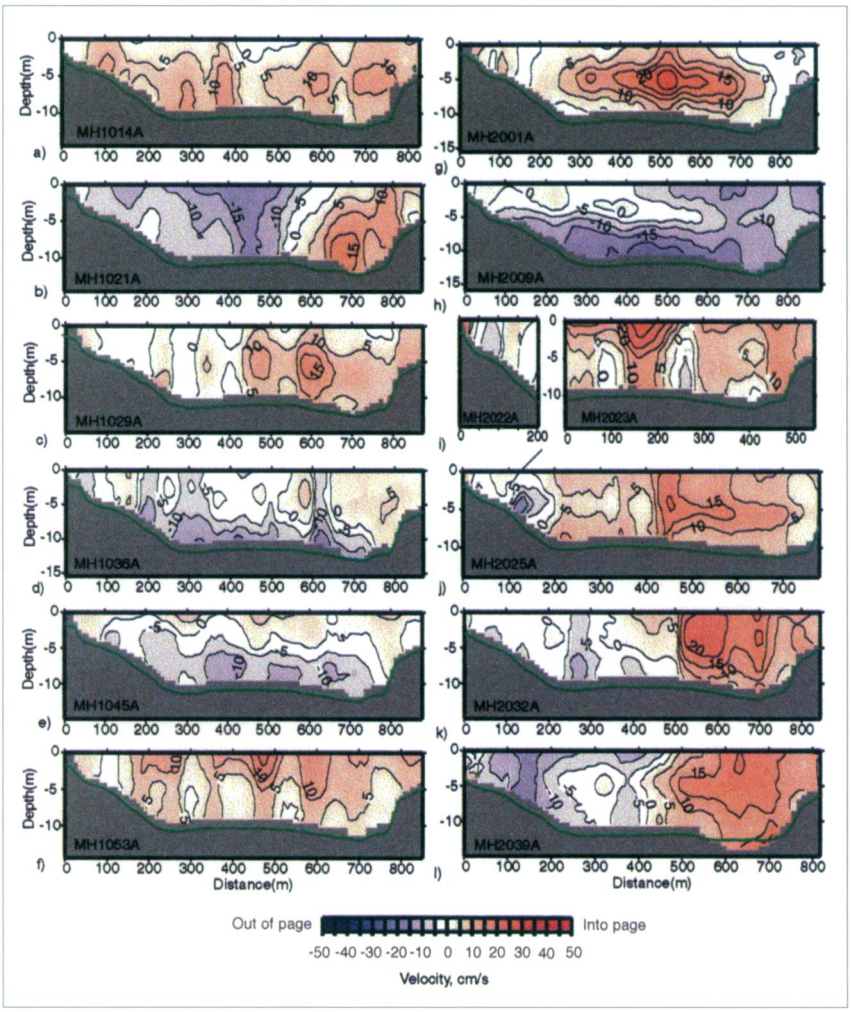

Figure 4. Similar series of contour plots of velocity magnitude normal to transect line as in Figure 3, but for transect line T2. Line T2 is located at the interface between MHB and the Sakonnet River. The cross-section is oriented with the view to the north such that west (east) is the left (right) side of the frame. Reds represent flow to the north, or currents entering MHB. Blues represent flow out of MHB, to the south. Frames (a–f) are from survey day 1. Frames (g–l) are from survey day 2. Frame (i) is split into two frames as the line was interrupted due to a passing ship.

inflow (> 80 cm/s) occupied an inclined region of the cross-section, extending from the deepest part of the channel (at ≈ 300 m along transect) up into shallower waters at the southeastern end of the transect. The region of maximum inflow at the surface occurs 400–600 m along the transect, running from the northwestern end of the line.

The occurrence of a reversed, outflow region during three different flood stages of the tide during the two survey days (e.g., Fig. 3i vs. 3n) highlights the repeatability in this aspect of exchange between MHB and Narragansett Bay. However, there are notable differences in the character of this outflow feature between the survey days that suggest a dependence on tidal amplitude. Data from the early stage of the flood (Fig. 3m) on day 2 show a weak inflow in the region where there was an outflow recorded on survey day 1 (Fig. 3b; e.g., at the bottom between 100–150 m along transect). However, during the mid- to late flood stages on day 2, this region of reversed flow is significantly larger than what was seen on survey day 1, occupying the entire water column from 0–200 m (Figs. 3h, 3i, 3n). Velocities in the outflow core reach 10–20 cm/s, which are significantly larger than those seen on survey day 1. Finally, the transition between inflow and outflow regions is remarkably sharp, occurring over a shear zone of roughly 50 m. This observation is reflected in the velocity contours (Fig. 3h) and is consistent with field observations recorded on survey day 2 in which neighboring lobster pots were seen to trend in opposite directions.

The timing of maximum currents relative to periods of high and low water is different on survey day 2. Maximum inflow velocities were observed on our first circuit at ≈ 7:00 on line T1, which was two hours prior to high water. While the actual timing of maximum inflow may have been even earlier, these data suggest the system is behaving more like a standing wave, where maximum inflow would occur ≈ 3 hours prior to high water. Measurements taken just prior to high water (Fig. 3i) show the inflow magnitudes have dropped off while the region of outflowing water has expanded to the southeast. The shear zone between the two flow structures also broadens (Fig. 3h vs. Fig. 3i). Velocity patterns recorded during the ebb stage of the tide do not show as coherent a spatial pattern as seen during the flood. Outflow during the ebb through T1 covers the entire cross-section, with weaker peak velocities of 50 cm/s on survey day 1 and 70–80 cm/s on survey day 2. Regions of more intense outflow within the deeper 2/3 of the cross-section appear to occupy the central region between 200–500 m along the transect line (Figs. 3f, 3k). On both survey days, regions of enhanced outflow appear earlier in the ebb and at shallower depths (< 10 m), situated at the southern end of line T1 (≈ 500–700 m along transect; Figs. 3e, 3j).

The MHB-Sakonnet River interface

The MHB system has two connections to the ocean. The smaller of these in terms of cross-sectional area (Table 1) is through transect T2 into the Sakonnet River. Just to south of our line T2 is the highly constricted SRN, which is characterized by extremely high water velocities (> 150 cm/s),

turbulent boils that are strikingly apparent on the water surface, and occasional standing waves. We chose a transect location to the north of the northern entrance to the SRN (Fig. 1, Table 1) in order to avoid such vigorous sampling conditions. Data from transect T2 are summarized in Figure 4. Instantaneous velocities through this cross-section peak at 20–25 cm/s and are far weaker than those recorded through T1. Lateral variability in flow is also recorded in the records for T2 from both sampling days. While the patterns are less striking than those recorded at T1, a similar structure is apparent in that northerly flows into MHB tend to occupy the eastern side of this cross-section (Figs. 4b, 4d, 4l, and 4m). Southerly, or ebb currents, tend to occur through the deeper and western portions of the cross-section (Figs. 4b, 4d, 4e, 4h, 4l, and 4m). A robust feature of these data is that horizontal shear is apparent in records for T2 from nearly all stages of the tidal cycle. Moreover, exchange through line T2 is periodically out of phase with trends recorded at line T1. Temporal variations in transport are discussed in more detail below.

The MHB–Taunton River interface

Figure 5 shows data from transect T4, which trends in a northwest to southeast direction and lies just south of the Brightman Street Bridge (Fig. 1). The orientation of flow through this cross-section tends to align with the channel. Peak speeds of 30–40 cm/s are recorded during the flood on sampling day 1 with lower amplitude tide (≈ 1 m) and reach 50 cm/s in the surface waters during the ebb. During survey day 2, flow rates are uniformly larger and exceed 50 cm/s over the majority of the cross-section during both flood and ebb. Spaulding and White (1990) report a low-frequency, layered flow in the Taunton River, which is apparent in the instantaneous velocities from the data set collected during survey day 1. Records from mid-flood (Fig. 5a) and mid-ebb (Fig. 5e) show a pattern of vertically sheared flow, with surface waters moving southward out of the estuary while deeper water moves northerly or back up the estuary. There is no evidence of layered flow in the instantaneous records from survey day 2.

Circulation near Brayton Point

Velocity data collected along transect T3, running southeast from Brayton Point, are shown in Figures 6–8 and summarized in Tables 2–3. This transect is interesting because the bathymetry varies from the northern shelf region (Fig. 1), where mean depths are constant at ≈ 5 m, to the deeper (≈ 16 m) and narrower shipping channel. This transect line presented a challenge because the prevailing southwesterly winds generate particularly steep, choppy seas in this region of MHB. While we were able to obtain relatively clean underway ADCP data sets on each of the other transects over all stages of the tide, this was not the case on T3. The underway ADCP data that we were able to collect at T3 indicate that flow on the northern shelf is variable and does not necessarily follow that observed in the channel. Figure 6 shows velocity contours for transitional periods between flood and ebb tides on both days and representative flows during mid-late flood conditions.

Figures 6a and 6c illustrate the strong vertical and lateral differences in flow that can exist along this cross-section. The most prominent feature is the strongly layered flow in the channel. Deep water moves northeastward towards the interface with the Taunton River, while shallow water moves southwestward. In Figure 6a, during the slack before flood stage of the tide, this layered flow exists in the channel, while currents on the northern shelf are weak and variable. The increase in tidal amplitude on day 2 appears to drive water on the shelf and at shallow levels within the channel in a more coherent fashion. During the early ebb (Fig. 6c), water over the entire cross-section above 5 m depth flows southwestward. Bottom water in the channel

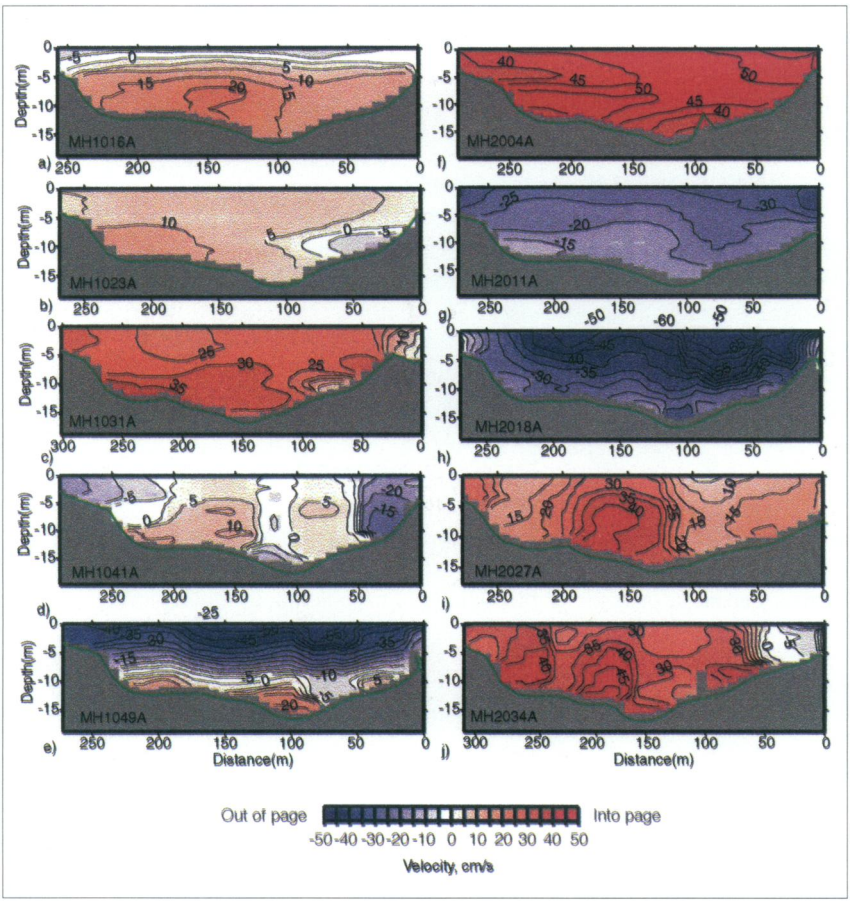

Figure 5. Similar series of contour plots of velocity magnitude normal to transect line as in Figure 3, but for transect line T4. Line T4 is located at the interface between MHB and the Taunton River. The cross-section is oriented with the view to the northeast into the Taunton River such that the left and right sides of the frame are to the northwest and southeast, respectively. Positive (red) flow is into the Taunton River. Negative (blue) values represent flow to the southwest (or ebb currents). Frames (a–e) are from survey day 1. Frames (f–j) are from survey day 2.

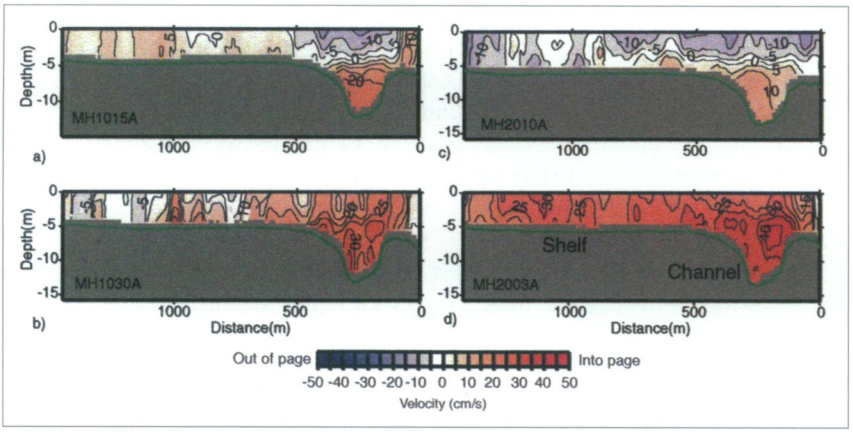

Figure 6. Velocity contour plots from transect line T3 on survey day 1 (a, b) and day 2 (c, d). Cross-sections are oriented with a view to the northeast, wth the left and right sides of the frames lying to the northwest and southeast, respectively. Contours highlight different flow patterns between the channel and the shallow shelf or shoal region spanning the northern and western regions of MHB. Frames (a) and (c) show stratified flow within the channel during the transitional periods between flood and ebb stages of the tide. Frames (b) and (d) show spatial patterns in flow during the late flood stage of the tide, with significantly higher flow rates on the northern shelf on day 2, which had a greater tidal range.

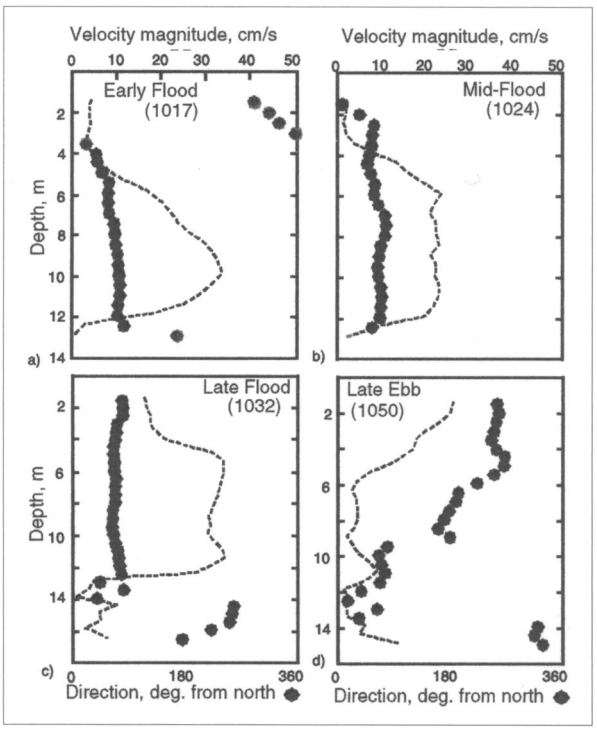

Figure 7. Plots of velocity magnitude (dashed line) and direction (circles) for data collected in the center of the channel at times series site (S1) on line T3 (Fig. 1). Data are from survey day 1. Profiles are averages from five minutes of data collection. The stages of the tide and the corresponding file numbers (Table 1) are shown.

is again flowing northeastward. During the flood on survey day 2, water on the northern shelf moves coherently northeastward (Fig. 6d), as opposed to the weak and variable currents recorded on survey day 1 (Fig. 6b).

Time-series data provide cleaner profiles of flow structures in the channel versus in the vicinity of Brayton Point because the vessel is anchored facing into the waves and bad data ensembles may be filtered. Time-averaged profiles of velocity magnitude and direction for site S1 at discrete points over the tidal cycle are shown in Figure 7. Time-series data from sites S1, S2, and S3 are summarized in Tables 2 and 3. Figure 7 shows the persistence of the vertical structure within the channel over the tidal cycle. Surface water (< 4 m) in the channel remains nearly stagnant during most of the flood, moving only weakly northward towards the end of the flood. Flow in the up-per 6 meters flows strongly (30 cm/s) to the south-southwest during the ebb. Alternatively, deeper water (> 6 m) moves strongly northward at 20–40 cm/s during the entire flood period, changing to a weak northerly flow during the ebb. Figure 8 compares the time variability in vertically averaged flow, projected to a northeast–southwest trend, within the surface and bottom waters of the channel relative to a laterally averaged flow on the shelf. On survey day 1, flow on the shelf is weakly northeastward during flood (≈ 5 cm/s), and switches to a weak southwestward flow during the ebb. The layered channel flow is apparent in Figure 8, as the surface water here varies with the tidal cycle, and the deep channel flow is persistently northeastward over most of the cycle. Instantaneous flow rates were higher on survey day 2 in both the channel (40 cm/s) and on the shelf (> 10 cm/s) (Table 3). Spatially averaged currents within each sub-region of line T3 vary with the tidal cycle, although the transition in surface outflow in the channel and over the shelf leads the transition to outflow in the deep channel (Fig. 8b). Interestingly, the northeastward components of the flow in both surface and bottom portions of the

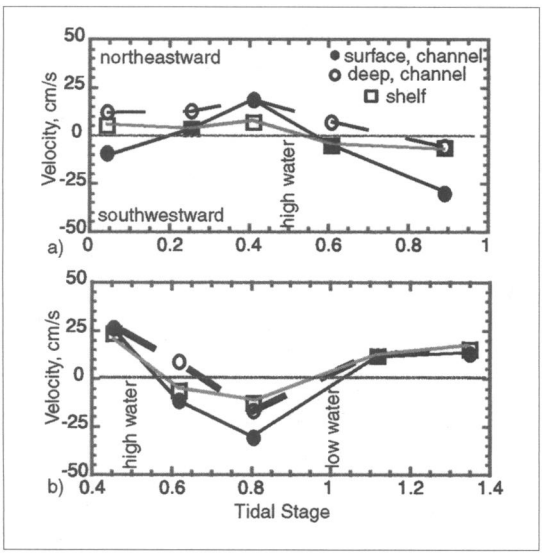

Figure 8. Plots of average velocity versus tidal stage for data from line T3 on days 1 (a) and 2 (b). Velocities have been projected to a 50° trend. Positive values are flow to the northeast (towards the head). Negative values are towards the mouth. On day 1, surface channel flow varies with the tide and deep flow is persistantly northeastward. On the shelf, flow is weak. Flow rates are higher on survey day 2.

channel, as well as along the shelf, are of equal magnitude during flood stages of the tide (Fig. 8b). As summarized in Table 3, flow at station S2 is predominantly eastward, or towards the channel, during the flood.

Basic differences in circulation through line T3 and the region south of Brayton Point during the two surveys are apparent when the data from Figure 8 are averaged over the tidal cycle. Residual flow within the channel and on the shelf are consistent with the patterns in the contours of instantaneous velocities shown in Figures 6a and 6c. On survey day 1, there is a net southwestward flow of surface water at 6.5 cm/s in the channel and a deep northeastward return flow at 7 cm/s. The pattern of layered residual flow is roughly similar on survey day 2, when average surface outflow in the channel is at 2 cm/s, with a deep residual inflow again of 7 cm/s. The greatest difference in residual flow is over the shelf, where net northeastward flow rates are ≈ 0.5 cm/s and > 5 cm/s on survey days 1 and 2, respectively.

Hydrographic data

CTD casts were taken on each transect and at each time series location (Fig. 1). Data were recorded just southeast of the channel midpoint on T1, on the deeper, eastern side of T2, within the channel on T3, and at the midpoint of T4. Figure 9 shows representative profiles for data collected at each of the MHB entrances. Representative profiles from T1 show a 2–4 °C drop in T across the upper 12 m of the water column. Below this level, T remains nearly constant. There is little stratification in the S field. Most of the profiles taken at site T2 show the water column to be well mixed vertically (Fig. 9d). During the ebb, a lens of warm water confined to the upper 2 m of the water column is recorded at site T2 (Fig. 9c). Profiles from the northern interface between MHB and the Taunton River are similar in structure to those at T1. While they are shifted towards warmer T, profiles at T4 show a region of thermal stratification in the upper 8–10 m of the water column, with nearly uniform T in the underlying water (Fig. 9e) over most of the tidal cycle. The depth of the transition from stratified to mixed water shallows to ≈ 4 m around the time of low water, or slack before flood (Fig. 9f). Profiles from T4 also show a 1–2 psu variation in S across this shallow, thermally stratified portion of the water column over most of the tidal cycle. A gradual, but larger 3 psu drop in S is recorded over the entire water column near the end of the ebb (Fig. 9f).

The ranges in average S and T recorded in the near-surface and near-bottom portions of the water column for each sampling site are shown in Figure 10. The distribution of these fields in T-S space suggests that a number of distinct end-member water sources may be identified within the MHB system. At one extreme is the relatively cool, salty bottom water recorded at T1, at the interface with the East Passage of Narragansett Bay. Another endmember would be the relatively warm, fresh, shallow water sampled at T4 coming from the outflow of the Taunton River. The water sampled at station S2 near Brayton Point represents still another distinct (in

T-S space) source within MHB. This water falls in between T1 bottom water and T4 surface water in terms of S. The distinguishing characteristic of this water source is that it is ≈ 2 °C warmer than T4 surface water. Figure 10 shows that water properties for surface versus bottom water are most similar for station T2, which lies just north of the turbulent mixing zone of the SRN. The warm extreme in the T2 surface range occurs during a brief period when water is moving southward from MHB into the SRN. During most of the tidal cycle, and particularly when flow is northward from the SRN into MHB, the water column at T2 is well mixed and has lower levels of thermal stratification than any other station.

Data collected at stations S1 and S2 provide information on the water in the direct vicinity of Brayton Point and some sense of the spatial and temporal evolution of the warm plume of water coming from the Brayton Point area. Surface water T at S2 remains nearly constant, just under 26 °C, over the tidal cycle. The more striking variation recorded in the profiles in

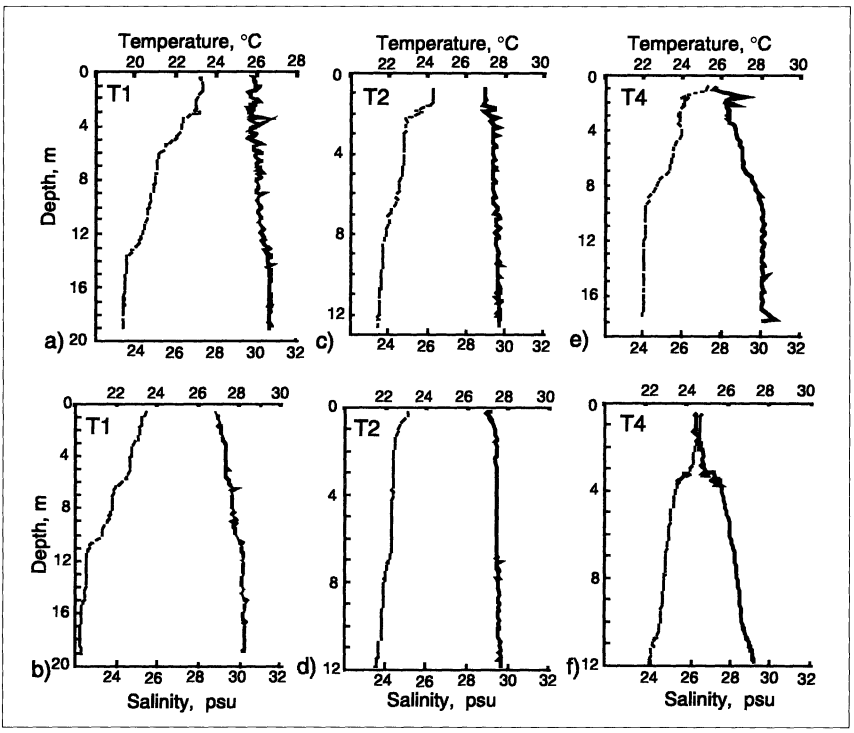

Figure 9. Profiles of salinity (thick solid line) and temperature (dashed line) collected along the entrances to MHB during survey day 1. The T1 plots are from slack before ebb (a) and slack before flood (b) periods and show thermal gradients in the upper 2/3 of the water colunm. The profiles for T2 are for mid-ebb (c) and slack before ebb (d) periods. Over most of the tidal cycle, the profiles at T2 are similar to (d), suggesting the water colunm is well mixed. Higher surface temperatures are seen during ebb (c). Profiles for T4 are from slack before ebb (e) and slack before flood (f) periods.

Figure 11 is the downward growth or expansion of a plug of relatively fresh, 26 °C water during the ebb. By late in the ebb, the upper 4 m of the water column measures uniformly at 25.9 °C and 28 psu. A similar temporal pattern is seen at station S3 during the ebb.

CTD profiles from within the shipping channel along transect T3 (S1) record the appearance of anomalously warm surface water during the flood (Fig. 12) when currents on the shelf are directed to the east-northeast or towards the S1 site (Tables 2 and 3, Fig. 8). The combination of ADCP and

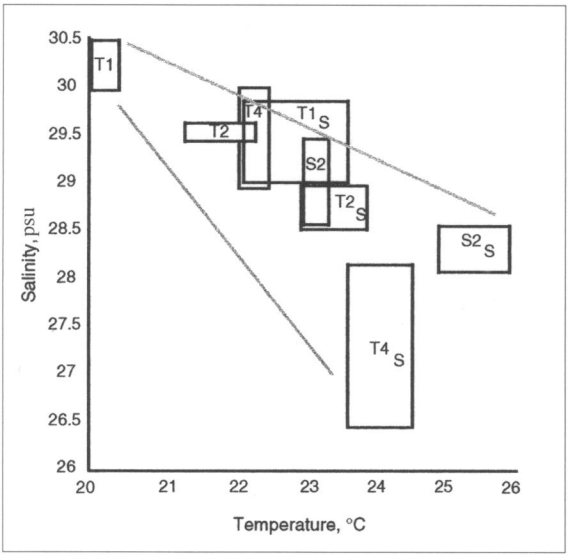

Figure 10. Plot summarizing the ranges (boxes) in salinity and temperature within surface (subscript S) and bottom waters over the tidal cycle. Data are shown for CTD casts from the mid-points of lines T1, T2, and T4. The highest temperatures are from $S2_s$.

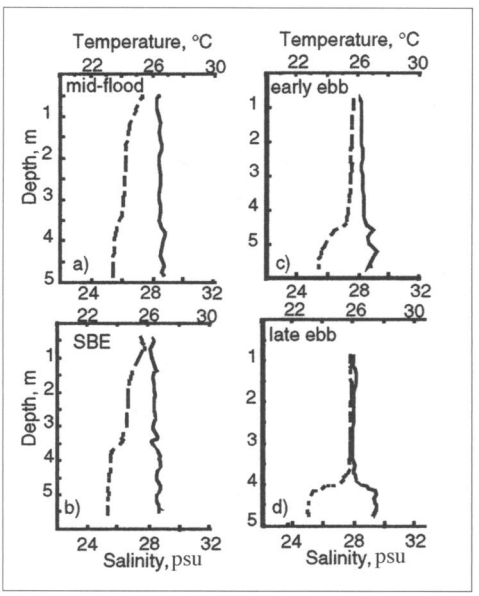

Figure 11. Profiles of temperature (dashed line) and salinity (solid line) from site S2, near Brayton Point on survey day 1. A plug of higher temperature water develops during the progression from flood to ebb conditions. Information on tidal stage is given.

T-S data suggest that warm water from near S2 is advected into the shipping channel during the flood before being carried southward during the ebb. Figure 12 shows that with the onset of the ebb, S1 surface T is reduced to a value that is closer to those recorded upriver at T4. Surface S at site S1 also drops during the progression of the ebb, reaching its lowest value of 27.5 psu at the end of the ebb tide.

Discussion

There are anthropogenic and natural characteristics of MHB that provide motivation for studies of circulation and transport in this system. One such factor is the dispersion of thermal energy from the Brayton Point Plant that is introduced to the northern shelf. These results suggest very different flushing scenarios for this region of MHB. During survey day 2 with the higher amplitude tide, there are stronger inflow or northeastward currents on the shelf that appear to carry warm water from site S2 towards the S1 channel location (Fig. 6, Table 3). There was also a relatively strong northeastward residual current that suggests warm waters are flushed towards the channel. During the lower amplitude tide on survey day 1, circulation on the shelf was weak and variable, with very weak residual flow magnitudes (< 1 cm/s) suggesting the flushing from site S2 was less efficient. One possible implication of this result that warrants further study is that, during larger amplitude tides, the warm plume from near S2 may be more efficiently carried eastward where it is mixed with water within the shipping channel before moving outward. Alternatively, during lower amplitude tides the warm water from the region near site S2 might remain confined along the northern MHB shore and follow a southwesterly trajectory, remaining closer to the western boundary of MHB. Such distinct dispersion pathways might influence the longer term thermal evolution, or flushing, of MHB.

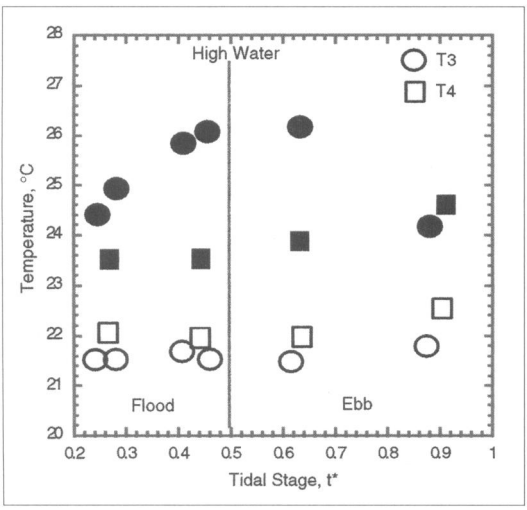

Figure 12. Averaged temperature for surface (filled) and bottom (open) waters of lines T3 (circles) and T4 (squares) over a tidal cycle. Data are from the center of T4 and in the channel for T3. A region of elevated temperature develops within the water column at T3, reaching a maximum near high water. Peak surface temperatures at T4 occur at the end of the ebb. Bottom water values are less variable.

A somewhat unique natural feature of the MHB system is that it has two connection points to the ocean, or two mouths. A goal of these surveys was a further understanding of how MHB exchanges water, in both a temporal and spatial sense, with both the East Passage of Narragansett Bay and the Sakonnet River. As shown above, data from the underway ADCP surveys provide detailed information on spatial variability in currents through each of the boundaries of MHB. These velocity data may also be integrated over the cross-sectional area of each transect to provide constraints on total volume flux, or transport of water through each of these boundaries. The variation in instantaneous transport over the tidal cycle recorded at lines T1, T2, and T4 is plotted in Figures 13 and 14. The largest volume flux is recorded through line T1. Values reach 3300 m^3/s and 6000 m^3/s on sampling days 1 and 2, respectively. Nearly doubling the tidal amplitude results in nearly double the transport. The plots show that exchange between MHB and the Sakonnet River through T2 is far more restricted, with peak transports that are a factor of 10 less than through T1. Transport values through T4 at the northern boundary of MHB are a factor of 4–5 less than through T1.

Results show interesting temporal variations in total transport through the MHB entrances. Figures 13 and 14 show the system is dominated by the M2 tide. The timing of maximum transport into MHB through T1 is different on the two survey days, occurring one hour prior to high water on day 1 with the lower amplitude tide. Maximum transport from MHB though T1 occurs mid-way between high and low water on survey day 2. Periods of zero transport coincide closely with times of high and low water. Both of these observations are more characteristic of a standing wave. The relative timing of transport through the different boundaries provides an indication of how MHB interacts with neighboring bodies of water. The variation in transport with time at lines T1 and T4 is nearly in phase. Figure 13 shows that each of these curves takes a dip during the flood, which is consistent with a double flood brought about by the interaction between the M_2 and M_4 tidal constituents (Spaulding and White 1990).

The complexity of exchange to and from MHB is reflected in the time variability in total transport through T2, relative to T1 . There are periods during both survey days when transport through T2 is out of phase with that recorded at T1. In Figure 13, there is a reversal in transport midway through the flood that aligns with similar features in the records from T1 and T4 that are most likely due to the M4 tidal constituent. There are also periods near the end of the flood and the end of the ebb when transport through T2 reverses direction relative to T1 (Figs. 13 and 14). One explanation is that the MHB-Sakonnet River interaction is dominated by the more efficient exchange through the T1 interface with the East Passage. A simple model explanation then is that during most of the flood MHB fills from both the East Passage and the Sakonnet River. However, late in the flood, MHB overfills relative to the Sakonnet River, creating a north-to-south gradient in sea-surface height that causes the flow through T2 to reverse direction to the

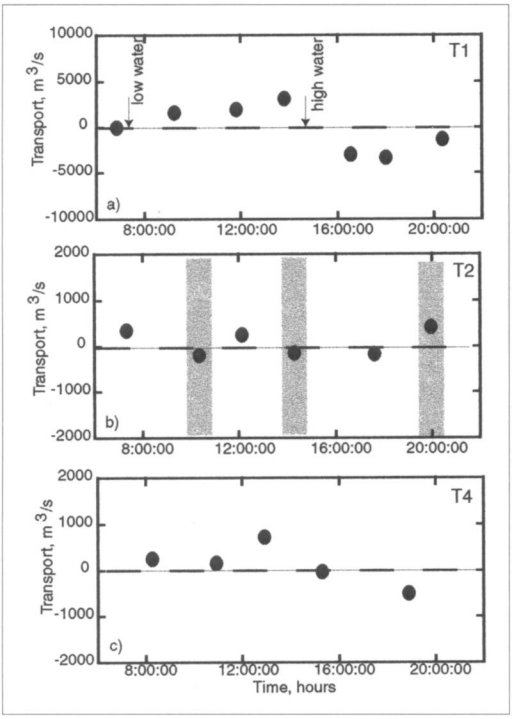

Figure 13. Plots of total transport through each of the entrances to MHB during survey day 1: a) T1, b) T2, and c) T4. The times of high and low water are shown in (a). Shaded regions in (b) indicate where transport through T2 is out of phase with line T1. Positive values rerpesent flow into MHB for T1 and T2, and flow from MHB into the Taunton River for T4.

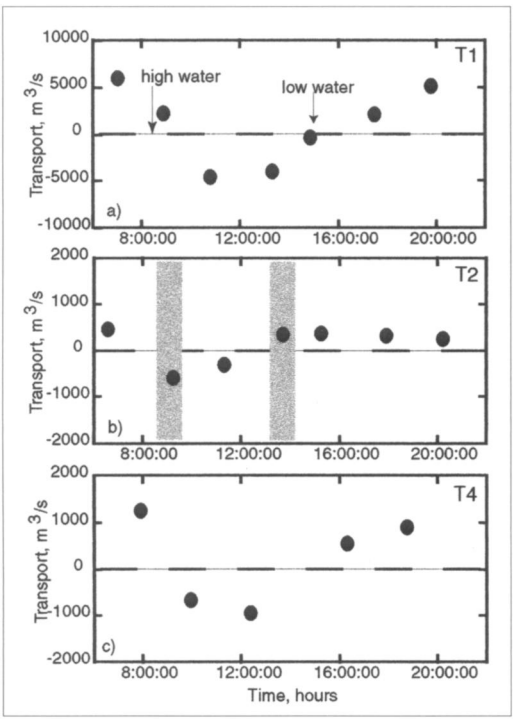

Figure 14. Similar series of plots as shown in Figure 13, but for survey day 2. Shaded regions in (b) show where transport through line T2 is out of phase with line T1. Transport values are higher on day 1, which is consistent with the larger tidal amplitude on day 2.

south. Similarly, during the majority of the ebb, water drains from MHB though both the T1 and T2 interfaces. MHB drains more efficiently through T1, and late in the ebb the system is set down relative to the Sakonnet River, creating a south-to-north gradient in sea surface elevation. This in turn drives a northerly transport of water through T2.

The total transport through the T2 interface is relatively small compared with the volume of water exchanged through T1 with the East Passage. However, because the SRN is such an efficient mixer, this tidal pumping that occurs between MHB and the SRN over the course of every M_2 cycle might have important implications for the thermal evolution of MHB. CTD profiles show that flow out of MHB through T2 can carry a lens of warm water that is confined to shallow levels. Such a tidal pump might pass this water column into the SRN during the early ebb, where the thermal energy is mixed downwards in the water column followed by the advection of the mixed water column back into MHB at the end of the ebb. With the subsequent onset of the flood, this mixed water column may in turn mix well into MHB. In this scenario, the tidal pumping between the MHB and the SRN mixes near-surface thermal energy down in the water column before sending it on a conveyor belt back into MHB.

Residual flow patterns are calculated from the instantaneous velocity data in order to characterize non-tidal exchange through the interfaces of

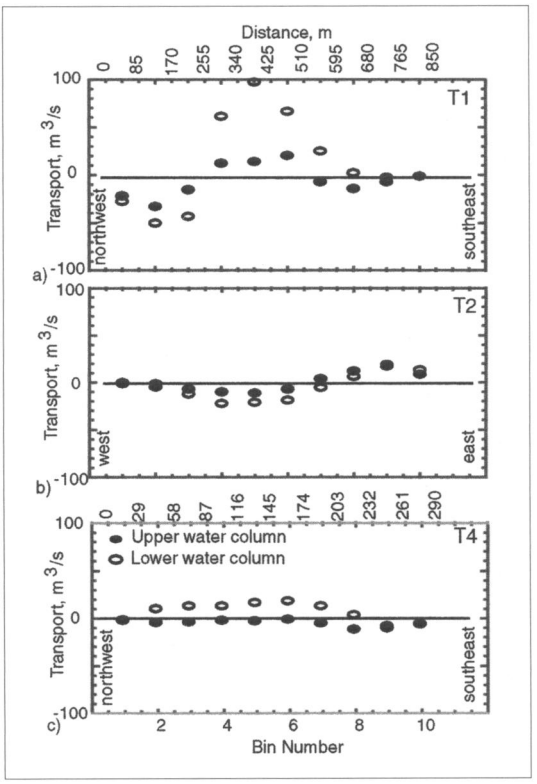

Figure 15. Plots of residual transport within 10 lateral bins across transect lines spanning the entrances to MHB for day 1: a) T1, b) T2, and c) T4. Dark circles represent values for data from the upper half of the water colunm. Open circles are values from data within bins defining the lower half of the water column. Bin widths are 85 m (a,b) and 29 m (c). Length scales for T1 and T2 are shown on the top of (a) and for T4 on the top of (c). Positive values are transport into MHB through T1 (a) and T2 (b) and into the Taunton River from MHB for T4 (c).

MHB. Figures 15 and 16 show vertical and lateral patterns in residual transport (q_R) through the two mouths (T1 and T2) and the head (T4) of MHB. As described in the methods section, q_R values are determined within 10 lateral bins located in the upper and lower halves of the water column to retain the detailed spatial information provided by the underway ADCP surveys. For example, there could be a vigorous net inflow and outflow through a transect line that sums to nearly zero when considering only the total net transport through a cross-section. The maximum values of q_R are recorded through line T1 on each survey day (80–100 m^3/s). It is interesting that the spatial structure in residual transport is similar on each day, despite the differences in tidal amplitude. Water moves into the MHB over the entire water column through the middle section of line T1, from roughly 250–600 m along track beginning at the northwestern end of the transect. A stronger net inflow is recorded in the bottom half of the water column. Two regions of net outflow occupy the edges of the cross-section. The stronger of these is at the northwestern end of the line, from 0–250 m along track, where outward q_R values peak at 50 m^3/s and 80 m^3/s in the lower water column on days 1 and 2, respectively. Maximum q_R values through line T2 reach 25 m^3/s and are lower than through T1. The characteristic lateral flow structure seen in the instantaneous records for line T2 shows up in the plots of residual

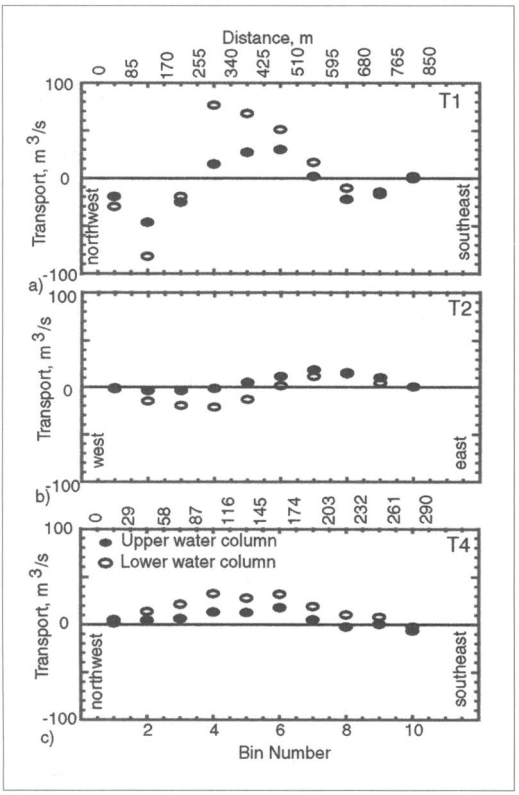

Figure 16. Similar plot of residual transport through lines T1, T2, and T4 as shown in Figure 15, but for survey day 2. Residual flow patterns are very similar to day 1 plots for T1 and T2.

transport, with net inflow and net outflow through eastern and western portions of the transect. The stronger outflow is through the lower half of the water column (Figs. 15b and 16b). Water moves towards MHB through the entire water column over the eastern 200 m and 350 m of the cross-section on days 1 and 2. The combination of the hydrographic data with the q_R estimates supports the conceptual model of a thermal pump in the area of line T2, as discussed above. The model suggests that near-surface thermal energy is mixed downwards into the water column within the Sakonnet River Narrows and then recycled back into MHB. The prevailing residual northerly transport along the eastern side of the transect identified on both survey days should serve as an efficient mechanism for advecting thermal energy that has been mixed downward in the water column back into MHB.

Plots of residual transport through T4 reveal more vertical structure than lateral structure through the head of MHB (Figs. 15c and 16c). A deep net inflow spans most of the cross-section on both days, with the strongest values ($\approx$ 35 m^3/s) situated in the central 100 m of the transect line. Relatively weaker surface outflow and inflow are recorded on days 1 and 2, with a slightly stronger outflow core on the southeastern end of the line on day 1. The lack of a stronger net surface outflow is likely due to the missed data coverage in the upper 1–2 m of the water column.

Conclusions

Results have been presented from hydrographic surveys conducted within MHB during summer conditions from August, 1996. ADCP data show that flow through each of the entrances to MHB exhibits significant horizontal and vertical structure. During the flood, flow into MHB from the East Passage of Narragansett Bay though transect T1 is concentrated in the southeastern 2/3 of the section, while a zone of stagnant or weakly ebbing water occupies the northwestern third of the cross-section. During the ebb, water moves uniformly out of MHB through T1. Similarly, data from transect T2 at the interface between MHB and the SRN show significant patterns of lateral shear, but over both flood and ebb stages of the tide. These results suggest that care should be taken in the placement of moorings for monitoring long-term flow and transport through the boundaries of MHB. Layered flow structures, with surface water moving out of the estuary and deeper water moving back into the system, were recorded through transects T4 and T3 in the northern portion of MHB where it meets the Taunton River.

Data on S and T support a model that includes three distinct water sources within MHB, including deep water from Narragansett Bay (cool, salty), surface water from the Taunton River (warm, fresh), and anomalously warm water from the shelf region near Brayton Point. The combination of ADCP and CTD data collected along T3 and at time series sites S1, S2, and S3 provide insight into processes operating within upper MHB. Flow rates for water on the northern shoals are generally a factor of 3–6 times smaller than flow rates through the channel. Currents tend to be southerly during ebb

and easterly during flood. A plug of warm water evolves at the S2 site over the ebb cycle of the tide that is ultimately advected during the flood to the east-northeast towards the vicinity of the shipping channel along line T3. The strength of this easterly flow and, presumably, the tendency for water from S2 to be flushed to the east during the flood and mixed into the channel, increase during the higher amplitude tide.

Exchange is dominated by flow through the interface between MHB and the East Passage of Narragansett Bay (T1), where peak transports reach 3300 m^3/s and 6000 m^3/s for low and high amplitude tides, respectively. Peak transport values through the boundary with the Sakonnet River (T2) are 10% of those recorded through the boundary with the East Passage. Interestingly, transport through T1 and T2 become out of phase during late stages of both the flood and the ebb. A simple model is suggested in which more efficient exchange of water through T1 causes MHB to become either set up or set down relative to the Sakonnet River towards the end flood and ebb, respectively. The resulting gradient in sea surface-height causes a reversal in transport through T2. Patterns in residual transport show significant lateral and vertical structure in the exchange of water through the mouths of MHB. Water moves into the system through the deep central portion of T1, and exits through relatively narrow regions at the edge of the cross-section. A persistent lateral structure in residual transport occurs through line T2, with a net outflow from MHB in the western, and primarily deeper, portion of the cross-section. Water enters MHB in a net sense through the eastern portion of the cross-section. Further study is required to better quantify spatial and temporal patterns of exchange from MHB and to better resolve the circulation patterns in the direct vicinity of Brayton Point, given various tidal, wind, and runoff conditions. In particular, it would be interesting to test the qualitative model suggested here that enhanced mixing south of line T2 combined with the net northerly flow of water along the eastern shore serves to pump thermal energy back into the bottom waters of MHB.

Acknowledgments

Rob Pockalny, William Deleo, and Dwight Coleman provided invaluable assistance during the long and often bumpy data collection cruises. We thank Dwight Coleman and family for providing sleeping quarters at their home on Hog Island, to allow for early starts. We also thank two anonymous reviewers for thorough and extremely helpful comments. This work was supported by the Bonnell Cove Foundation and the Brayton Point Power Plant.

Literature Cited

Bergondo, D. 2004. Examining the processes controlling water column variability in Narragansett Bay: Time series data and numerical modeling. Ph.D. Dissertation. University of Rhode Island, Narragansett, RI. 187 pp.

Bergondo, D., and C. Kincaid. 2003. Observations and modeling on circulation and mixing processes within Narragansett Bay. EOS Transactions, American Geophysical Union, Fall Meeting.

Candela, J., R.C. Beardsley, and R. Limeburner. 1990. Removing tides from ship-mounted ADCP data, with application to the Yellow Sea. Pp. 258–266, *In* G.F. Appell and T. B. Curtin (Eds.). Proceedings of the IEEE Fourth Working Conference on Current Measurements. Institute of Electrical and Electronic Engineering. New York, NY.

Candela, J., R.C. Beardsley, and R. Limeburner. 1992. Separation of tidal and subtidal currents in ship-mounted acoustic Doppler current profiler observations. Journal of Geophysical Research 97:769–788.

Deacutis, C. 1999. Nutrient Impacts and Signs of Problems in Narragansett Bay. Pp. 7–23, *In* M. Kerr (Ed.). Nutrients and Narragansett Bay: Proceedings of a Workshop on Nutrient Removal from Wastewater Treatment Facilities. RI Sea Grant, Narragansett, RI. 64 pp.

Deleo, W. 2001. Investigation of the physical mechanisms controlling exchange between Mount Hope Bay and the Sakonnet River. M.Sc. Thesis. University of Rhode Island, Narragansett, RI.

Foreman, M.G.G., and H.J. Freeland. 1991. A comparison of techniques for tide removal from ship-mounted acoustic Doppler measurements along the southwest coast of Vancouver Island. Journal of Geophysical Research 96:17,001–17,021.

Geyer, W.R., and R. Signell. 1990. Measurements of tidal flow around a headland with a shipboard acoustic Doppler current profiler. Journal of Geophysical Research 95:3189–3197.

Goodrich, D.M. 1988. On meteorologically induced flushing in three US East Coast estuaries. Estuarine, Coastal, and Shelf Science 26:111–121.

Gordon, R.B., and M.L. Spaulding. 1987. Numerical simulations of the tidal and wind-driven circulation in Narragansett Bay. Estuarine, Coastal, and Shelf Science 24:611–636.

Hawk, J.D. 1998. The role of the North Atlantic oscillation in winter climate variability as it relates to the winter–spring bloom in Narragansett Bay. M.Sc. Thesis in Oceanography. University of Rhode Island, Narragansett, RI. 148 pp.

Hicks, S.D. 1959. The physical oceanography of Narragansett Bay. Limnology and Oceanography 4:316–327.

Keller, A.A., G. Klein-MacPhee, and J. St. Onge Burns. 1999. Abundance and distribution of ichthyoplankton in Narragansett Bay, Rhode Island, 1989–1990. Estuaries 22:149–163.

Kincaid, C., R. Pockalny, and L. Huzzey. 2003. Spatial and temporal variability in flow and hydrography at the mouth of Narragansett Bay. Journal of Geophysical Research 108:3218–3235.

Levine, E.R., and K.E. Kenyon, 1975. The tidal energetics of Narragansett Bay. Journal of Geophysical Research 80:1683–1688.

Munchow, A., R.W. Garvine, and T.F. Pfeiffer. 1992. Subtidal currents from a shipboard acoustic Doppler current profiler in tidally dominated waters. Continental Shelf Research 12:499–515.

Pilson, M. 1985a. On the residence time of water in Narragansett Bay. Estuaries 8:2–14.

Pilson, M. 1985b. Annual nutrient cycles and chlorophyll in Narragansett Bay, RI. Journal of Marine Research 43:849–873.

Rosenberger, K. 2001. Circulation patterns in Rhode Island Sound: Constraints from a bottom mounted acoustic Doppler current profiler. M.Sc. Thesis in Oceanography. University of Rhode Island, Narragansett, RI. 226 pp.

Shonting, D.H. 1969. Rhode Island Sound square kilometer study 1967: Flow patterns and kinetic energy distribution. Journal of Geophysical Research 74:3386–3395.

Simpson, J.H., E.G. Mitchelson-Jacob, and A.E. Hill. 1990. Flow structure in a channel from an acoustic Doppler current profiler. Continental Shelf Research 10:589–603.

Spaulding, M.L., and F.M. White. 1990. Circulation dynamics in Mount Hope Bay and the Lower Taunton River. Pp. 494–510, *In* R.T. Cheng (Ed.). Residual Currents and Long-term Transport, Coastal and Estuarine Studies, 38, Springer-Verlag, New York, NY.

Valle-Levinson, A., and K.M.M. Lwiza. 1995. The effects of channels and shoals on exchange between the Chesapeake Bay and the adjacent ocean. Journal of Geophysical Research 100:18,551–18,563.

Valle-Levinson, A., J.M. Klinck, and G.H. Wheless. 1996. Inflows/outflows at the transition between a coastal plain estuary and the coastal ocean. Continental Shelf Research 16:1819–1847.

Valle-Levinson, A.V., C. Li, T.C. Royer, and L. Atkinson. 1998. Flow patterns at the Chesapeake Bay entrance. Continental Shelf Research 18:1157–1177.

Weisberg, R.H. 1972. The Net Circulation in the West Passage of Narragansett Bay. M.Sc. Thesis. University of Rhode Island, Narragansett, RI. 90 pp.

Weisberg, R.H. 1976. The non-tidal flow in the Providence River of Narragansett Bay: A stochastic approach to estuarine circulation. Journal of Physical Oceanography 6:721–734.

Weisberg, R.H., and W. Sturges. 1976. Velocity observations in the West Passage of Narragansett Bay, a partially mixed estuary. Journal of Physical Oceanography 6:345–354.

Wong, K-C., and A. Münchow. 1995. Buoyancy forced interaction between estuary and inner shelf: Observation. Continental Shelf Research 15:59–88.